The 8th European Congress on Computational Methods in Applied Sciences and Engineering
ECCOMAS Congress 2022
5-–9 June 2022, Oslo, Norway

ROBUST TOPOLOGY OPTIMIZATION OF STATIC SYSTEMS WITH UNILATERAL FRICTIONAL CONTACT

T. SCHMIDT[1], B. KRIEGESMANN[2] AND R. SEIFRIED[1]

[1] Hamburg University of Technology, Institute of Mechanics and Ocean Engineering, Germany, timo.schmidt@tuhh.de and robert.seifried@tuhh.de

[2] Hamburg University of Technology, Institute for Structural Mechanics in Lightweight Design, Germany, benedikt.kriegesmann@tuhh.de

Key words: Robust topology optimization, Contact, Uncertainty

Abstract. In this paper a robust topology optimization algorithm for linear elastic structures in unilateral contact is presented. The deformation of the linear elastic structure is constrained by support structures that are modeled with the help of Signorini's contact conditions. The contact conditions in turn are enforced with the augmented Lagrangian approach. Doing so, the robust optimization considers uncertainties at the support such as manufacturing tolerances and its local friction behavior. Due to high numerical costs in robust optimization, the first-order second-moment approach is used to approximate the mean and variance of the objective. This approximation results in minimal additional costs to approximate the mean, the variance and their gradients. Consequentially, a gradient-based optimization algorithm can be used to minimize a weighted sum of both. The results show that the presented approach indeed improves the robustness with respect to uncertain contact conditions compared to a deterministic optimization.

1 INTRODUCTION

Robust topology optimization allows that defined uncertainties are taken into account during the optimization. This is crucial, since an optimized component can be highly sensitive against small environmental variations. These can occur, for example, through manufacturing tolerances, local material inhomogeneities or modeling assumptions such as the usage of ideally rigid, friction-less and clearance-free bearings in the model. In order to guarantee that the optimized component performs as expected, its sensitivity against such unknown must be minimized. This is of utmost importance at the support, since Dirichlet boundary conditions cannot capture the unilateral behavior between the support and the component. Due to this observation, the work of Strömberg and Klarbring [6] was developed, where an efficient framework for topology optimization with unilateral contact constraints is presented. However, this framework did not allow to consider uncertainties.

A general drawback of robust topology optimization is its numerical performance. In fact, its costs can exceed today's computational limits quickly, which is why, a first-order second-moment approach (FOSM) is used in this paper. FOSM is a linear approximation of the first two stochastic moments in particular the mean and variance. Thus, gradient information can

be provided so that deterministic optimization algorithms can be used for robust topology optimization. Furthermore, the linear approximation leads to small additional numerical costs, so that a robust design can be found in reasonable time.

2 Robust Topology Optimization

Robust Topology Optimization applies the concepts of robust design optimization. An overview of these concepts is provided in Zang et al. [7]. In doing so, the design variables $\boldsymbol{y}$ and the random vector $\boldsymbol{z}$ are introduced. Next, the objective $f(\boldsymbol{y}, \boldsymbol{z})$ is replaced by its mean μ_f and its standard deviation σ_f. The robust optimization problem states

$$\begin{aligned} &\min_{\boldsymbol{y}} \mu_f(\boldsymbol{y}) + \kappa\sigma_f(\boldsymbol{y}), \\ &\text{s.t.} \begin{cases} \boldsymbol{g}(\boldsymbol{y}) \leq \boldsymbol{0} \\ \boldsymbol{h}(\boldsymbol{y}) = \boldsymbol{0} \end{cases} \end{aligned} \tag{1}$$

where $\kappa > 0$ is a weighting factor, $\boldsymbol{g}$ are inequality constraints and $\boldsymbol{h}$ are equality constraints. Consequentially, the mean and the standard deviation or the variance of f must be computed. They are defined as

$$\mu_f = \int_{-\infty}^{\infty} f(\boldsymbol{z}) p(\boldsymbol{z}) d\boldsymbol{z} \quad \text{and} \quad \sigma_f^2 = \int_{-\infty}^{\infty} (f(\boldsymbol{z}) - \mu_f)^2 p(\boldsymbol{z}) d\boldsymbol{z}, \tag{2}$$

where $p(\boldsymbol{z})$ is a defined probability density function.

Monte Carlo simulations can be used to approximate both, but this leads to tremendous numerical costs in structural optimization. Nonetheless, the mean and the variance can be approximates as

$$\mu_f(\boldsymbol{y}) \approx \sum_{i=1}^{n_{\text{MCS}}} f(\boldsymbol{z}_i) \quad \text{and} \quad \sigma_f^2 \approx \frac{1}{n_{\text{MCS}} - 1} \sum_{i=1}^{n_{\text{MCS}}} (f(\boldsymbol{z}_i) - \mu_f)^2, \tag{3}$$

where $\boldsymbol{z}_i$ is a set of randomly sampled variables and n_{MCS} is the total number of Monte Carlo samples.

Another way to approximate the mean and the variance provides the first-order second-moment method (FOSM). It was introduced by Cornell [1] in 1969 and is based on a Taylor series of the mean and variance. Using this approach, the mean is

$$\mu_f \approx f(\boldsymbol{\mu}_{\boldsymbol{z}}), \tag{4}$$

where $\boldsymbol{\mu}_{\boldsymbol{z}}$ is the mean of the random vector $\boldsymbol{z}$. Next, the variance is

$$\sigma_f^2 \approx \sum_{i=1}^{n} \sum_{j=1}^{n} \frac{\partial f(\boldsymbol{\mu}_{\boldsymbol{z}})}{\partial z_i} \frac{\partial f(\boldsymbol{\mu}_{\boldsymbol{z}})}{\partial z_j} \text{cov}(z_i, z_j), \tag{5}$$

where n is the number of random quantities and $\text{cov}(z_i, z_j)$ is an entry of the covariance matrix, see e.g. [2, 3].

3 System Equations

The system equations for a linear elastic body in contact can be derived from the equilibrium equations of the finite element method and are given as

$$\boldsymbol{K}\boldsymbol{d} + \boldsymbol{f}_{\text{con}} - \boldsymbol{q} = \boldsymbol{0}, \tag{6}$$

where $\boldsymbol{K}$ is the stiffness matrix, $\boldsymbol{d}$ is the displacement field, $\boldsymbol{f}_{\text{con}}$ are the nodal contact forces and $\boldsymbol{q}$ are the external forces acting at the linear elastic body. The stiffness matrix is calculated based on the modified SIMP approach [5], so that the elements stiffness E_i depends on its normalized density $\varphi_i \in [0, 1]$

$$E_i = E_{\min} + \varphi_i^p (E_{\max} - E_{\min}), \tag{7}$$

where the penalization factor is $p = 3$. The Young's modulus of the void elements is defined by $E_{\min}$, while $E_{\max}$ is the modulus of the material.

In order to compute the nodal contact forces $\boldsymbol{f}_{\text{con}}$, Signorini's contact condition must be met. A detailed derivation of the condition inside a contact-constraint topology optimization algorithm is provided in the work of Stromberg and Klarbring [6]. In summary, the following non-smooth contact condition must be fulfilled at all contact nodes

$$\Phi^A = -\xi^A + \max(0, \xi^A + r(g^A - \boldsymbol{n}^A \cdot \boldsymbol{d}^A)) = 0, \tag{8}$$

where ξ^A is the contact force of the A-th contact node, $\boldsymbol{n}^A$ is the associated contact normal direction, $\boldsymbol{d}^A$ is the nodal displacement and g^A is the initial distance between the A-th node of the elastic body and the support. Finally, $r > 0$ is a factor increasing numerical performance.

The Eq. (6) and Eq. (8) are used to derive the KKT condition, that must be meet to solve the non-linear contact system equations. They read

$$\boldsymbol{h}_{\text{c}}(\boldsymbol{d}, \boldsymbol{\xi}, \boldsymbol{\varphi}) = \begin{Bmatrix} \boldsymbol{K}(\boldsymbol{\varphi})\boldsymbol{d} + \boldsymbol{f}_{\text{con}}(\boldsymbol{\xi}) - \boldsymbol{q} \\ \boldsymbol{\Phi}(\boldsymbol{d}, \boldsymbol{\xi}) \end{Bmatrix} = \boldsymbol{0}, \tag{9}$$

$$\boldsymbol{h}_{\text{c}}(\boldsymbol{x}, \boldsymbol{\varphi}) = \underbrace{\begin{bmatrix} \boldsymbol{K}(\boldsymbol{\varphi}) & (\boldsymbol{N} + \{\mu \boldsymbol{T}\})^{\text{T}} \\ \dfrac{\partial \boldsymbol{\Phi}(\boldsymbol{x})}{\partial \boldsymbol{d}} & \dfrac{\partial \boldsymbol{\Phi}(\boldsymbol{x})}{\partial \boldsymbol{\xi}} \end{bmatrix}}_{\boldsymbol{J}_{\text{c}}} \underbrace{\begin{bmatrix} \boldsymbol{d} \\ \boldsymbol{\xi} \end{bmatrix}}_{\boldsymbol{x}} - \underbrace{\begin{bmatrix} \boldsymbol{q} \\ \boldsymbol{\Phi}_{\text{c}}(\boldsymbol{x}) \end{bmatrix}}_{\boldsymbol{r}_{\text{c}}} = \boldsymbol{0}, \tag{10}$$

where $\boldsymbol{J}_{\text{c}}$ is the contact Jacobian, $\boldsymbol{x}$ is the state vector and $\boldsymbol{r}_{\text{c}}$ holds the external forces $\boldsymbol{q}$ and the state independent part of the contact law. Note that, the lower rows of Eq. (10) depend on the current state of the contact nodes. In doing so, a non-linear solver such as a line-search algorithm can be used to calculate the solution of displacement field $\boldsymbol{d}$ and the contact forces $\boldsymbol{\xi}$.

4 Robust Compliance Optimization Problem

The compliance of a contact-constrained linear-elastic structure is minimized and is defined as

$$c = \boldsymbol{q}^T \boldsymbol{d} = \underbrace{\begin{bmatrix} \boldsymbol{q} \\ \boldsymbol{0} \end{bmatrix}^{\text{T}}}_{\boldsymbol{r}} \boldsymbol{x}. \tag{11}$$

The design variables are the normalized densities $\boldsymbol{\varphi}$ of the finite element discretization, so that the optimization problem reads

$$\begin{aligned} &\min_{\boldsymbol{\varphi}} \mu_c(\boldsymbol{\varphi}) + \kappa\sigma_c(\boldsymbol{\varphi}) \\ &\text{s.t.} \begin{cases} \boldsymbol{h}_\mathrm{c}(\boldsymbol{\varphi}, \boldsymbol{x}) = \mathbf{0}, \\ V(\boldsymbol{\varphi}) - V_0 \leq 0, \\ \mathbf{0} \leq \boldsymbol{\varphi} \leq \mathbf{1}. \end{cases} \end{aligned} \tag{12}$$

The system equations of the contact problem $\boldsymbol{h}_\mathrm{c}$ as well as a volume constraints must be fulfilled. The initial gap g^A between the A-th contact node and the support structure as well the nodal friction coefficient μ^A are assumed to be random. Hence, the random vector consists of both

$$\boldsymbol{z} = \begin{bmatrix} \boldsymbol{z}_g \\ \boldsymbol{z}_\mu \end{bmatrix} \in \mathbb{R}^{2n_\mathrm{con}}, \tag{13}$$

where the subvector $\boldsymbol{z}_g = [g^1, \dots, g^{n_\mathrm{con}}]^\mathrm{T}$ holds all random gaps and $\boldsymbol{z}_\mu = [\mu^1, \dots, \mu^{n_\mathrm{con}}]^\mathrm{T}$ holds all random friction coefficients of the contact nodes. The described setup is shown in Fig. 1, where the surface of the support structure scatters. The ideal form of the support is shown in gray and locally described by the mean values $\mu^A_{\boldsymbol{z}_g}$ and $\mu^A_{\boldsymbol{z}_\mu}$ of the random variables. Next to that, the actual random support structure is shown, where the gap and friction coefficient of the A-th contact node are z^A_g and z^A_μ.

Last, the scattering of the random variables must be defined. The random variables $\boldsymbol{z}_g$ and $\boldsymbol{z}_\mu$ are assumed to be spatially correlated by an exponential correlation function. Therefore, a set of normal distributed random variables $\tilde{\boldsymbol{z}}$ is generated. Each independent variable $\tilde{z}_i$ has a mean of zero and variance is one. The exponential correlation function for the contact nodes i and j is

$$C_{i,j} = \exp\left(-\frac{||\boldsymbol{d}^i - \boldsymbol{d}^j||^2}{l_c^2}\right), \tag{14}$$

where l_c is the correlation length. If the standard deviation of the random variables $\sigma(\boldsymbol{z})$ is given, the covariance is

$$\mathrm{cov}(z_i, z_j) = C_{i,j}\sigma(z_i)\sigma(z_j), \tag{15}$$

and the covariance $\mathrm{cov}(z_i, z_j)$ is stored in the covariance matrix $\boldsymbol{\Sigma}_{\boldsymbol{z}}$. Consequentially, the random contact gaps $\boldsymbol{z}_g$ and the random friction coefficients $\boldsymbol{z}_\mu$ are defined as

$$\boldsymbol{z}_g = \boldsymbol{\Sigma}^{\frac{1}{2}}_{\boldsymbol{z}_g}\tilde{\boldsymbol{z}}_g + \boldsymbol{\mu}_{\boldsymbol{z}_g} \quad \text{and} \quad \boldsymbol{z}_\mu = \boldsymbol{\Sigma}^{\frac{1}{2}}_{\boldsymbol{z}_\mu}\tilde{\boldsymbol{z}}_\mu + \boldsymbol{\mu}_{\boldsymbol{z}_\mu}. \tag{16}$$

Note, the random gap z^A_g and the friction coefficient z^A_μ of the A-th node are independent of each other, while both the gaps and the friction coefficients are correlated to their neighbor gaps and friction coefficients.

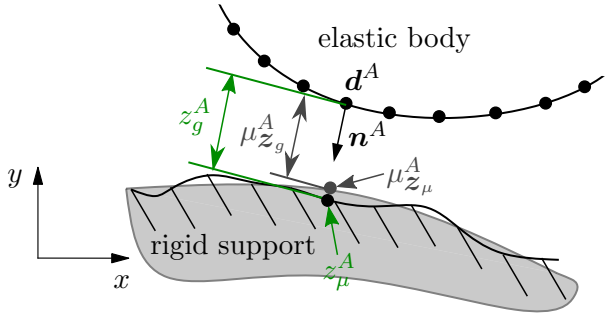

Figure 1: A linear elastic body unilaterally constrained by a non-ideal rigid support.

4.1 Objective

In contrast to the standard compliance optimization, it is not trivial to calculate the objective with FOSM. The FOSM approximation states that the mean of the compliance is

$$\mu_c(\boldsymbol{\varphi}) \approx c(\boldsymbol{x}(\boldsymbol{\varphi}), \boldsymbol{\mu_z}). \tag{17}$$

However, the standard deviation must be derived from the variance approximation of Eq. (5), where the partial derivative of the compliance $c(\boldsymbol{\mu_z})$ with respect to the random variables $\boldsymbol{z}$ is needed. The computation of this partial derivative is costly, which is why an adjoint variable $\boldsymbol{\zeta}$ is introduced.

If the adjoint $\boldsymbol{\zeta}$ is chosen such that

$$\left(\boldsymbol{r}^{\mathrm{T}} - \boldsymbol{\zeta}^{\mathrm{T}} \boldsymbol{J}_{\mathrm{c}}(\boldsymbol{x}(\boldsymbol{\mu_z}))\right) = \boldsymbol{0}, \tag{18}$$

the derivative simplifies to

$$\frac{\partial c(\boldsymbol{x}, \boldsymbol{\mu_z})}{\partial z_i} = -\boldsymbol{\zeta}^{\mathrm{T}} \left(\frac{\partial \boldsymbol{J}_{\mathrm{c}}(\boldsymbol{x}(\boldsymbol{\mu_z}))}{\partial z_i} \boldsymbol{x}(\boldsymbol{\mu_z}) - \frac{\partial \boldsymbol{r}_{\mathrm{c}}(\boldsymbol{\mu_z})}{\partial z_i} \right). \tag{19}$$

Note, the adjoint equation (18) is independent of z_i, meaning that the adjoint is the same for all partial derivatives of $\boldsymbol{z}$. As a result, only one additional set of linear equations must be solved to calculate the FOSM approximation of the variance of the compliance. Next, the variance is calculated as stated in Eq. (5) and the objective of the defined optimization problem given by Eq. (12) is approximated with FOSM. The optimization problem using FOSM reads

$$\begin{aligned} \min_{\boldsymbol{\varphi}} \quad & \underbrace{c(\boldsymbol{x}, \boldsymbol{\mu_z})}_{\mu_c^{\mathrm{FOSM}}} + \kappa \underbrace{\sqrt{\sum_{i=1}^{2n_{\mathrm{con}}} \sum_{j=1}^{2n_{\mathrm{con}}} \frac{\partial c(\boldsymbol{x}, \boldsymbol{\mu_z})}{\partial z_i} \frac{\partial c(\boldsymbol{x}, \boldsymbol{\mu_z})}{\partial z_j} \mathrm{cov}(z_i, z_j)}}_{\sigma_c^{\mathrm{FOSM}}} \\ \text{s.t.} \quad & \begin{cases} \boldsymbol{h}_{\mathrm{c}}(\boldsymbol{\varphi}, \boldsymbol{x}) = \boldsymbol{0}, \\ V(\boldsymbol{\varphi}) - V_0 \leq 0, \\ \boldsymbol{0} \leq \boldsymbol{\varphi} \leq \boldsymbol{1} \end{cases} \end{aligned} \tag{20}$$

where $\dfrac{\partial c(\boldsymbol{x}, \boldsymbol{\mu_z})}{\partial z_i}$ is defined by Eq. (19) and the covariance is obtained from the covariance matrix

$$\boldsymbol{\Sigma_z} = \begin{bmatrix} \boldsymbol{\Sigma}_{\boldsymbol{z}_g} & \mathbf{0} \\ \mathbf{0} & \boldsymbol{\Sigma}_{\boldsymbol{z}_\mu} \end{bmatrix}. \tag{21}$$

If the weighting factor κ is $\kappa = 0$, the robust optimization problem simplifies to the deterministic contact-constrained topology optimization problem of Strömberg and Klarbring [6].

4.2 Gradient of the approximated Objective

In order to use gradient-based optimization algorithms, the derivative of the objective with respect to the design variables must be computed. Therefore, the objective of Eq. (20) is subdivided into its two parts and the derivatives are derived separately.

The first part corresponds to the approximation of the mean of the compliance. It turns out, that the same adjoint system known from Eq. (18) must be solved to avoid computing the costly derivative $\dfrac{\partial \boldsymbol{x}(\boldsymbol{\mu_z})}{\partial \varphi_e}$. If the adjoint equation is chosen such that

$$\left(\boldsymbol{r}^{\mathrm{T}} - \tilde{\boldsymbol{\zeta}}^{\mathrm{T}} \boldsymbol{J}_{\mathrm{c}}(\boldsymbol{x}(\boldsymbol{\mu_z}))\right) = \mathbf{0}, \tag{22}$$

no further computational costs occur for the first part of the derivative, since this equation has been solved to calculate the standard deviation. The derivative reads

$$\frac{\partial \tilde{c}(\boldsymbol{x}, \boldsymbol{\mu_z})}{\partial \varphi_e} = -\boldsymbol{\zeta}^{\mathrm{T}} \left(\frac{\partial \boldsymbol{J}_{\mathrm{c}}(\boldsymbol{x}(\boldsymbol{\mu_z}))}{\partial \varphi_e} \boldsymbol{x}(\boldsymbol{\mu_z}) \right). \tag{23}$$

The derivative of the Jacobian with respect to the elements density is

$$\frac{\partial \boldsymbol{J}_{\mathrm{c}}(\boldsymbol{x}(\boldsymbol{\mu_z}))}{\partial \varphi_e} = \begin{bmatrix} \dfrac{\partial \boldsymbol{K}(\boldsymbol{\varphi})}{\partial \varphi_e} & \mathbf{0} \\ \mathbf{0} & \mathbf{0} \end{bmatrix}, \tag{24}$$

where the derivative of the stiffness matrix with respect to the e-th element is the derivative of the elements local stiffness matrix including the SIMP approach of Eq. (7). A more detailed derivation can be found in [6].

For the second part of the objective, the approximation of the standard deviation $\sigma_{\mathrm{c}}^{\mathrm{FOSM}}$ must be derived with respect to the elements densities as well. Consequentially, it is necessary to compute

$$\begin{aligned} \frac{\partial \sigma_{\mathrm{c}}^{\mathrm{FOSM}}}{\partial \varphi_e} &= \frac{\partial}{\partial \varphi_e} \sqrt{\sum_{i=1}^{2n_{\mathrm{con}}} \sum_{j=1}^{2n_{\mathrm{con}}} \frac{\partial c(\boldsymbol{x}, \boldsymbol{\mu_z})}{\partial z_i} \frac{\partial c(\boldsymbol{x}, \boldsymbol{\mu_z})}{\partial z_j} \operatorname{cov}(z_i, z_j)} \\ &= \frac{1}{2\sigma_{\mathrm{c}}^{\mathrm{FOSM}}} \frac{\partial}{\partial \varphi_e} \underbrace{\left(\sum_{i=1}^{2n_{\mathrm{con}}} \sum_{j=1}^{2n_{\mathrm{con}}} \frac{\partial c(\boldsymbol{x}, \boldsymbol{\mu_z})}{\partial z_i} \frac{\partial c(\boldsymbol{x}, \boldsymbol{\mu_z})}{\partial z_j} \operatorname{cov}(z_i, z_j) \right)}_{(\sigma_{\mathrm{c}}^{\mathrm{FOSM}})^2}. \end{aligned} \tag{25}$$

It turns out, that the computational costs of Eq. (25) are reduced to a minimum, if the chain rule is applied inside the double sum. As a result, the partial derivatives with respect to $\boldsymbol{z}$ are replaced by the adjoint Eq. (19). In combination with two additional adjoint equations and the corresponding adjoint variables $\boldsymbol{\eta}$ and $\boldsymbol{\gamma}$, the FOSM approximation of the variance reads

$$\left(\tilde{\sigma}_{\mathrm{c}}^{\mathrm{FOSM}}\right)^2 = \left(\sigma_{\mathrm{c}}^{\mathrm{FOSM}}\right)^2 - \boldsymbol{\eta}^{\mathrm{T}} \underbrace{\boldsymbol{h}_{\mathrm{c}}(\boldsymbol{x}(\boldsymbol{\mu}_{\boldsymbol{z}}))}_{=\mathbf{0}} - \underbrace{\left(\boldsymbol{r}^{\mathrm{T}} - \boldsymbol{\zeta}^{\mathrm{T}} \boldsymbol{J}_{\mathrm{c}}(\boldsymbol{x}(\boldsymbol{\mu}_{\boldsymbol{z}}))\right)}_{=\mathbf{0}^{\mathrm{T}}} \boldsymbol{\gamma}. \tag{26}$$

As a result, the derivative simplifies to

$$\frac{\partial \sigma_{\mathrm{c}}^{\mathrm{FOSM}}}{\partial \varphi_e} = \frac{\partial \tilde{\sigma}_{\mathrm{c}}^{\mathrm{FOSM}}}{\partial \varphi_e} = \frac{1}{2\sigma_{\mathrm{c}}^{\mathrm{FOSM}}} \left[- \boldsymbol{\eta}^{\mathrm{T}} \frac{\partial \boldsymbol{J}_{\mathrm{c}}(\boldsymbol{x}(\boldsymbol{\mu}_{\boldsymbol{z}})}{\partial \varphi_e} \boldsymbol{x}(\boldsymbol{\mu}_{\boldsymbol{z}}) + \boldsymbol{\zeta}^{\mathrm{T}} \frac{\partial \boldsymbol{J}_{\mathrm{c}}(\boldsymbol{x}(\boldsymbol{\mu}_{\boldsymbol{z}})}{\partial \varphi_e} \boldsymbol{\xi} \right], \tag{27}$$

where the following adjoint equations must be satisfied

$$\begin{aligned} \mathbf{0} = &- \sum_{i=1}^{2n_{\mathrm{con}}} \sum_{j=1}^{2n_{\mathrm{con}}} \left[\mathrm{cov}(z_i, z_j) \boldsymbol{\zeta}^{\mathrm{T}} \left(\frac{\partial c(\boldsymbol{x}, \boldsymbol{\mu}_{\boldsymbol{z}})}{\partial z_j} \frac{\partial \boldsymbol{J}_{\mathrm{c}}(\boldsymbol{x}(\boldsymbol{\mu}_{\boldsymbol{z}}))}{\partial z_i} + \frac{\partial c(\boldsymbol{x}, \boldsymbol{\mu}_{\boldsymbol{z}})}{\partial z_i} \frac{\partial \boldsymbol{J}_{\mathrm{c}}(\boldsymbol{x}(\boldsymbol{\mu}_{\boldsymbol{z}}))}{\partial z_j} \right) \right] - \dots \\ &\dots \boldsymbol{\eta}^{\mathrm{T}} \boldsymbol{J}_{\mathrm{c}}(\boldsymbol{x}(\boldsymbol{\mu}_{\boldsymbol{z}}), \end{aligned} \tag{28}$$

$$\begin{aligned} \mathbf{0} = \boldsymbol{J}_{\mathrm{c}}(\boldsymbol{x}(\boldsymbol{\mu}_{\boldsymbol{z}}) \boldsymbol{\gamma} + &\sum_{i=1}^{2n_{\mathrm{con}}} \sum_{j=1}^{2n_{\mathrm{con}}} \left[\mathrm{cov}(z_i, z_j) \left(\frac{\partial c(\boldsymbol{x}, \boldsymbol{\mu}_{\boldsymbol{z}})}{\partial z_j} \left(\frac{\partial \boldsymbol{J}_{\mathrm{c}}(\boldsymbol{x}(\boldsymbol{\mu}_{\boldsymbol{z}})}{\partial z_i} \boldsymbol{x}(\boldsymbol{\mu}_{\boldsymbol{z}}) - \frac{\partial \boldsymbol{r}_{\mathrm{c}}}{\partial z_i} \right) + \dots \right. \right. \\ &\left. \left. \dots \frac{\partial c(\boldsymbol{x}, \boldsymbol{\mu}_{\boldsymbol{z}})}{\partial z_i} \left(\frac{\partial \boldsymbol{J}_{\mathrm{c}}(\boldsymbol{x}(\boldsymbol{\mu}_{\boldsymbol{z}})}{\partial z_j} \boldsymbol{x}(\boldsymbol{\mu}_{\boldsymbol{z}}) - \frac{\partial \boldsymbol{r}_{\mathrm{c}}}{\partial z_j} \right) \right) \right]. \end{aligned} \tag{29}$$

Note, Eq. (27) is derived by observing, that the following partial derivatives are zero

$$\frac{\partial \boldsymbol{r}}{\partial \varphi_e} = \mathbf{0}, \quad \frac{\partial \boldsymbol{r}_{\mathrm{c}}}{\partial \varphi_e} = \mathbf{0}, \quad \frac{\partial^2 \boldsymbol{r}_{\mathrm{c}}}{\partial z_i \partial \varphi_e} = \mathbf{0} \quad \text{and} \quad \frac{\partial^2 \boldsymbol{J}_{\mathrm{c}}(\boldsymbol{x}(\boldsymbol{\mu}_{\boldsymbol{z}})}{\partial z_i \partial \varphi_e} = \begin{bmatrix} \mathbf{0} & \mathbf{0} \\ \mathbf{0} & \mathbf{0} \end{bmatrix}. \tag{30}$$

Finally, the derivative of the objective with respect to the design variables $\boldsymbol{\varphi}$ is defined as the sum of Eq. (23) and Eq. (27). It reads

$$\begin{aligned} \frac{\partial (\mu_c^{\mathrm{FOSM}} + \kappa \sigma_c^{\mathrm{FOSM}})}{\partial \varphi_e} = &\boldsymbol{\zeta}^{\mathrm{T}} \left(\frac{\partial \boldsymbol{J}_{\mathrm{c}}(\boldsymbol{x}(\boldsymbol{\mu}_{\boldsymbol{z}}))}{\partial \varphi_e} \boldsymbol{x}(\boldsymbol{\mu}_{\boldsymbol{z}}) \right) + \dots \\ &\dots \frac{\kappa}{2\sigma_{\mathrm{c}}^{\mathrm{FOSM}}} \left[- \boldsymbol{\eta}^{\mathrm{T}} \frac{\partial \boldsymbol{J}_{\mathrm{c}}(\boldsymbol{x}(\boldsymbol{\mu}_{\boldsymbol{z}}))}{\partial \varphi_e} \boldsymbol{x}(\boldsymbol{\mu}_{\boldsymbol{z}}) + \boldsymbol{\zeta}^{\mathrm{T}} \frac{\partial \boldsymbol{J}_{\mathrm{c}}(\boldsymbol{x}(\boldsymbol{\mu}_{\boldsymbol{z}}))}{\partial \varphi_e} \boldsymbol{\gamma} \right], \end{aligned} \tag{31}$$

where the adjoint equations (18), (28)and (29) must be satisfied.

4.3 Gradient of the Volume Constraint

The volume constraint was introduced in Eq. (12) and its derivative with respect to the density of the e-th element is

$$\frac{\partial V(\boldsymbol{\varphi})}{\partial \varphi_e} = V_e, \tag{32}$$

where V_e is the volume of the e-th element. The sensitivity of the volume constraint is independent of the design variables.

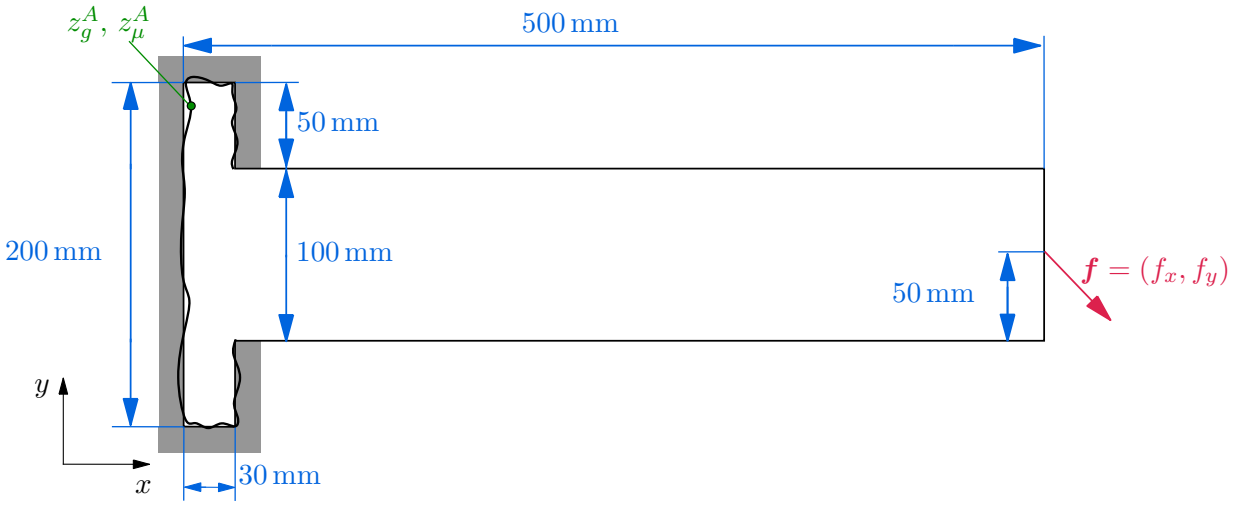

Figure 2: Cantilever beam with the concept of form closure.

Parameter	Meaning	Value
$E_{\min}$	min. Young's Modulus	1 MPa
$E_{\max}$	max. Young's Modulus	210000 MPa
$r_{\min}$	truncation radius of filter	10.5 mm
l_{corr}	correlation length	25 mm
κ	objective's weighting factor	3

Table 1: Parameters of the optimization.

5 Numerical Examples

The introduced robust optimization algorithm is applied to a cantilever beam as shown in Fig. 2. The cantilever beam is hold in place by the contact support structures on the left hand side and a vertical force of $f_y = -490.5\,\text{N}$ is applied on the right hand side. The geometry of the contact support structures and the local friction coefficients are considered to be random. The contact gaps are normally distributed with zero mean and a standard deviation of 30 µm. The friction coefficients are uniformly distributed between 0.15 and 0.25. The material parameters of the beam as well as the optimization parameters are given in table 1. The domain is discretized into 6026 elements, which corresponds to 75 contact nodes. Thus, the robust topology optimization considers 150 uncertain parameters.

5.1 Optimization results

The results of the robust optimization and the non-robust approach are shown in Fig. 3. They are obtained by optimizations that started from a uniform density distribution of $\varphi_i = 0.49$ and 1000 optimization iterations have been computed. Figures 3a and 3b show the resulting topology of the robust and non-robust compliance optimization. Both optimized domains have the same strut positioning inside the beam, while the topology inside the flange is different. The robust optimized domain has more material inside the flange and the contact areas with the support

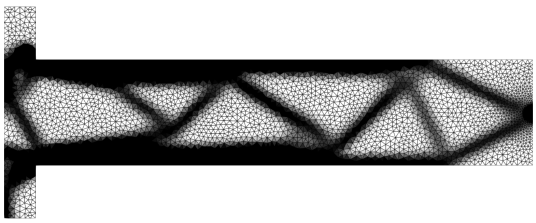

(a) Robust optimized topology ($\kappa = 3$).

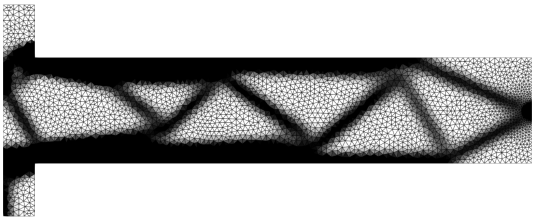

(b) non-robust optimized topology ($\kappa = 0$).

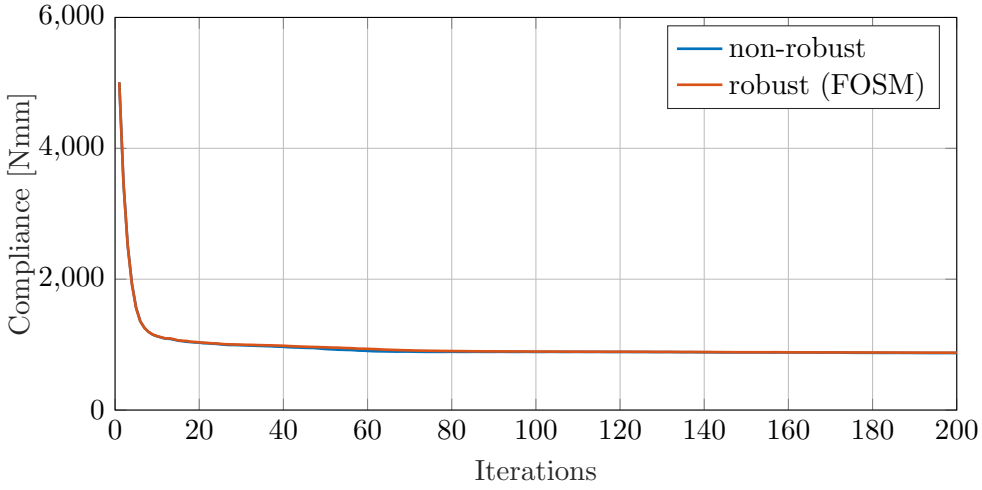

(c) Compliance of robust and non-robust optimization.

Figure 3: Optimization results for frictional contact-constrained optimization.

structure are wider.

Figure 3c shows the progress of the compliance over the first 200 iterations and convergence is observed. The compliance of the robust design is 877 Nmm, while the non-robust approach leads to a compliance of 871 Nmm. The final compliance of the robust design is 867 Nmm and about 0.6 % higher than the compliance of the non-robust approach with 862 Nmm. It is to be expected, that the non-robust topology optimization leads to a smaller compliance, since increasing the robustness comes at the costs of increasing the average compliance.

The performance of the robust contact-constrained topology optimization approach is analyzed with the help of the Monte Carlo Simulations. Therefore, 7000 random samples of contact gaps and friction coefficients are sampled and the compliance for the robust and non-robust final topologies are computed. It turns out, that the used sliding friction approach leads to poor convergence of the non-linear contact problem and sometimes even divergence is observed. The tangential contact force of a contact node is

$$\xi_t^A = z_\mu^A \xi^A. \tag{33}$$

The convergence issues are observed, because samples with high deformed contact support structures enforce high contact forces, which in turn leads to high and non-physical tangential forces.

Therefore, Coulomb's law considering a stick and slip case must be used to compute the Monte Carlo samples. Hence, the tangential contact force of a contact node reads

$$\xi_t^A = \min(z_\mu^A \xi^A, f_t^A), \tag{34}$$

where f_t^A is the tangential force acting at the contact node. Using Coulomb's law, the non-linear contact problem is solved without further problems and the compliance is computed for all samples. However, Coulomb's law is not applicable to the FOSM approach, since the resulting tangential contact function depends only indirectly on the friction coefficient. As a result, all partial derivatives with respect to the random friction coefficients cannot be determined. Due to that necessary modification, the results of the robust topology optimization cannot be used to determine the accuracy of the FOSM approach. Nonetheless the Monte Carlo samples show, that the robust approach reduces the standard deviation of the compliance.

The Monte Carlo simulation lead to similar average values of the compliance for both topologies. The robust topology has an average compliance of 887 Nmm, while the non-robust topology has a compliance of 882 Nmm. The obtained average values are higher than the values obtained by the optimization, since different friction laws are used. However, the Monte-Carlo simulation shows that the standard deviation of the robust optimized design is about 3 % smaller, than the standard deviation of the non-robust topology design. Thus, the robust design approach using FOSM results in a less sensitive topology, even though a different and more realistic tangential contact law has been used for the Monte Carlo samples.

6 Conclusion

In this work, the contact-constrained topology optimization framework of Strömberg and Klarbring [6] is extended to robust topology optimization. The presented approach considers uncertainties at the contact support structure, such as imperfect geometry and the local friction behavior, which are unavoidable in real world applications due to manufacturing tolerances. The robust optimization problem is efficiently solved using the first-order second-moment method and the compliance is minimized. As shown in the numerical example, the risk of potential failure of the component is reduced, since the sensitivity of the optimized topology against the defined uncertainty is reduced. The presented algorithms are implemented in the in-house code TOptiMuM solving 2D and 3D contact-constrained optimization problems.

7 Acknowledgement

The current work is a part of the research training group "Simulation-Based Design Optimization of Dynamic Systems Under Uncertainties" (SENSUS) funded by the state of Hamburg within the Landesforschungsförderung under project number LFF-GK11.

REFERENCES

[1] Cornell C.A. Structural safety specifications based on second- moment reliability analysis. *IABSE Rep Work Commiss.* (1969) **4**:235–245

[2] Haldar A., Mahadevan S. Probability, reliability and statistical methods in engineering design, 1. Auflage edn. Wiley, New York, 1999

[3] Kriegesmann B., Lüdeker J., Robust compliance topology optimization using the first-order second-moment method. *Structural and Multidisciplinary Optimization.* (2019) **60**:269–286

[4] Schuëller G.I., Valdebenito M. Reliability-based optimization - an overview. *Comput Technol Rev.* (2010) **1**:121–155.

[5] Sigmund, O.: Morphology-based black and white filters for topology optimization. *Structural and Multidisciplinary Optimization.* (2007) **33**:401–424

[6] Strömberg N., Klarbring A., Topology optimization of structures in unilateral contact. *Structural and Multidisciplinary Optimization.* (2010) **41**:57–64

[7] Zang T.A., Hemsch M.J., Hilburger M.W., Kenny S.P., Luckring J.M., Maghami P., Padula S.L., Stroud W.J. Needs and opportunities for uncertainty-based multidisciplinary design methods for aerospace vehicles. *Tech. Rep. NASA/TM-2002-211462*, National Aeronautics and Space Administration Langley Research Center, (2002)